Scientia Iranica B (2021) 28(3), 1271–1283

Sharif University of Technology
Scientia Iranica
Transactions B: Mechanical Engineering
http://scientiairanica.sharif.edu

Anisotropic finite element modelling of traumatic brain injury: A voxel-based approach

H. Hoursan[a], F. Farahmand[a,b], M.T. Ahmadian[a,*], and S. Masjoodi[c]

a. *Department of Mechanical Engineering, Sharif University of Technology, Tehran, Iran.*
b. *RCBTR, Tehran University of Medical Sciences, Tehran, Iran.*
c. *Department of Medical Physics and Biomedical Engineering, School of Medicine, Tehran University of Medical Sciences (TUMS), Tehran, Iran.*

Received 22 September 2019; received in revised form 31 July 2020; accepted 19 October 2020

KEYWORDS
3D head model;
Traumatic brain injury;
Finite element;
Anisotropy;
Heterogeneity.

Abstract. A computationally efficient 3D human head finite element model was constructed. The model includes the mesoscale geometrical details of the brain including the distinction between white and grey matter, sulci and gyri, the ventricular system, foramen magnum, and cerebrospinal fluid. The heterogeneity and anisotropy from diffusion tensor imaging data were incorporated by applying a one-to-one voxel-based correspondence between diffusion voxels and finite elements. The voxel resolution of the model was optimized to obtain a trade-off between reduced computational cost and higher geometrical details. Three sets of constitutive material properties were extracted from the literature to validate the model against intra-cranial pressure and relative motion test data within the brain. The model exhibited good agreement at pressure tests in frontal and occipital lobes with peak pressure magnitudes of only 8% and 6% higher, which occurred 0.5–3 ms earlier than those of the experimental curves at coup and countercoup sites, respectively. In addition, evaluation of the relative displacement at six locations within the brain indicated acceptable agreement with experimental data. The performance of the authors' model exhibited the highest overall score compared to several previous models, using the correlation and analysis rating method.

1. Introduction

Traumatic Brain Injury (TBI) affects almost 180–250 per 100,000 people in western countries every year, with a wide range of symptoms from death to temporary and long-term disability leading to invisible and visible loss of societal productivity. Biomechanical study of the TBI is still in its primary stage [1]. A vast literature of experimental and numerical research has focused on developing a better understanding of tissue response to external stimuli. Experimental approaches have often attempted to replicate real-life impact conditions using postmortem human subjects under laboratory conditions (see e.g. [2–4]). Such approaches have led to the advance of various macroscale criteria such as the HIC (Head Injury Criterion) and HIP (Head Impact Power) which relate a macroscale measure of the external stimuli (i.e. acceleration, velocity, impact energy, etc.) to damage, in terms of injury severity at tissue level. However, while cadaveric experiments address the phenomenological aspect of damage, they fail to provide any information regarding the mechanistic aspect of damage at tissue and sub-tissue levels.

*. *Corresponding author.*
E-mail addresses: Hesam.hoursan74@student.sharif.edu (H. Hoursan); Farahmand@sharif.edu (F. Farahmand); Ahmadian@sharif.edu (M.T. Ahmadian); Sadeghmasjoodi@gmail.com (S. Masjoodi).

doi: 10.24200/sci.2020.54280.3685

Along with rapid development of computational technology, numerical models with various degrees of complexity have emerged over the last several decades. These models range from simplified models of a human head with 20,000 elements to more accurate models containing 2 million elements [5], aiming to provide stress/strain distribution in various regions of the human brain subjected to external stimuli. As the computational cost of Finite Element (FE) models increases with anatomical accuracy, the accepted trade-off for reduced computational time has been a major challenge. The ultimate purpose of FE models is to combine accurate representations of the head and brain anatomy with sophisticated material properties to simulate deformation patterns and obtain tissue level mechanical parameters, such as stress and strain, within the brain tissue. These mechanical parameters may be extracted and used as injury predictors [6–15].

Recent studies on the mechanical properties of brain tissue have been greatly influenced by its anisotropic behaviour, especially within the white matter [16,17]. This has been illustrated using Diffusion-MRI, fiber tractography [18], and by histological observations of the tissue [19]. In particular, several experimental studies have shown that white matter tissue displays considerably [20–22] or marginally [23] higher stiffness along the axonal tracts. In addition to the direction-dependence, the mechanical properties within the white matter have been considered region-dependent (i.e. heterogeneous) [21,23]. This heterogeneity is mainly rooted in the spatially variable architecture, volume fraction, caliper, and orientation of axonal fibers [17,21,23] in different regions (structures) of the white matter, such as corpus callosum, corona radiata, etc.

While several 3D FE models have been proposed in the literature, few have attempted to incorporate the anisotropy and heterogeneity of material properties within the brain [24]. The inclusion of anisotropy data has often led to various complications leading to the reduced efficiency of the FE models. In addition, due to the dimensional difference between the baseline geometrical models and the original source of anisotropic field data, the few anisotropic models have often relied on scaling techniques and approximations to connect voxel-based anisotropy data and the FEs of the model [24,25]. Furthermore, most existing models employ a simplified geometry of the brain to meet the requirements of surface contact between adjacent regions. The simplified geometry is often the result of surface fitting and smoothing of contact surfaces between adjacent regions (e.g. CSF and Skull). While these simplifications often lead to loss of important tissue detail (e.g. sulci, gyri, ventricles, etc.), a considerable amount of literature has focused on the skull-brain boundary conditions (see e.g. [26–29]), as well as the effect of impact direction [14], leading to contradictory results. On the other hand, patient specific models require a direct algorithm to derive FE mesh from T1 data [30]. Therefore, the previously proposed FE models entail several major insufficiencies in geometrical accuracy, incorporation of anisotropy and heterogeneity, patient specificity, and computational cost-effectiveness. In order to gain a deeper insight into the damage mechanisms of TBI as a result of macroscopic loading at various orientations and intensities, more efficient anisotropic macroscale models are required.

This study aims to develop and validate a computationally inexpensive FE human head model (the SUTHM, Sharif University of Technology Head Model) including anisotropy and heterogeneity from DTI data using a voxel-based mesh generation approach, suitable for patient specific modelling. Two major challenges of FE-based head modeling are tackled:

1. Accurately reproducing the geometry of an original scan;
2. Accurate inclusion of patient specific anisotropy and heterogeneity of white matter into the FE model.

In order to obtain a FE model with acceptable computational cost, the voxel resolution of the model is optimized to obtain a trade-off between reduced computational cost and geometrical details. The one-to-one correspondence between the FEs and DTI voxels allows for incorporation of anisotropy and heterogeneity. The main orientation and dispersion factor from DTI voxels are inserted into the FE models in the form of global elemental orientation and dispersion matrices. Three sets of hyperelastic parameters are assigned to the model from previous experiments. The model is then validated against intra-cranial pressure by applying a frontal impact, and evaluating the coup and countercoup response at two opposite points in the frontal and occipital lobes. Finally, the model is validated against the relative motion data of 6 points within the brain using CORA (Correlation and Analysis Rating Method) to evaluate the similarity of two curves, and the results are compared to some other existing FE head models.

2. Methods

2.1. MRI/DTI data acquisition

T1 and Diffusion Weighted Images (DWI) were obtained from a 25-year-old male healthy subject. The original data included 176 slices with 1 mm in-plane resolution. Imaging was performed using a single shot imaging pulse sequence with gradient sectors in 12 directions and b-value = 1000 s/mm^2. The obtained

slices were realigned by selecting a single coronal slice as reference. A linear mapping algorithm was used to adjust the size matrix of coronal sections to the reference image through displacement, rotation and scaling. Normalization was carried out by adjusting the pixel intensity of all voxels in grey scale to meet the optimum values based on Eq. (1):

$$I_N = (I - \min)\frac{\text{new max} - \text{new min}}{\max - \min} + \text{new min}, \quad (1)$$

where I denotes the numerical pixel intensity, I_N is the normalized intensity, min and max are the old minimum and maximum intensity in greyscale, and new min and new max are the new minimum and maximum pixel intensity in greyscale, respectively. In order to smooth the pixel matrix and enhance the Signal to Noise Ratio (SNR), a linear Gaussian kernel was applied to all coronal sections. Finally, a Statistical Parametric Mapping (SPM) method was used to classify and extract 4 tissues (i.e. skull, CSF, grey matter, white matter) via the SPM toolbox. Each voxel was assigned to a class with the highest probability based on the probability map of each class (Figure 1).

Exploratory DTI was utilized to register DTI data onto T1 images and to extract the 4D diffusion tensors for all voxels of the white matter [18]. A method similar to that explained by Karimi et al. [31] was employed with distortion/subject motion correction, and rigid co-registration. The results were verified by using the DTIFIT tool of the diffusion toolbox in FSL software package (Oxford Centre for Functional MRI of the Brain, FMRIB [32]). The diffusion tensor was then calculated for all voxels using the weighted nonlinear least square method [31]. The eigenvalue and eigenvector maps were extracted for all voxels using custom MATLAB scripts. Negative eigenvalues were set to zero to guarantee the positive definitiveness of the diffusion tensor.

2.2. FE model

The FE model of SUTHM was initially developed with four different voxel sizes of 1, 1.5, 2, and 4 mm for the means of parametric study. The resulting number of cubic elements in each model is shown in Table 1. The mesoscale morphological details of the tissue, such as sulci and gyri, on the cortex of the grey matter, ventricles, and foramen magnum were captured by all models. In order to avoid increased local stresses at the contact surfaces and the zigzagging effect [30], smoothing was applied to surface elements at skull-CSF, and CSF-brain contacts. However, in order to avoid loss of element quality, the smoothing was applied partially to keep the Jacobian of all surface elements above 0.8. The contact between adjacent regions of skull-CSF, CSF-grey matter, and grey-matter-white matter was modelled with a tie constraint between nodes on adjacent voxels. This mode of interaction led to more reliable results, while other modes, such as frictional or frictionless contact, resulted in excessive boundary deformations and invalid results. Linear hexahedral elements with reduced integration (C3D8R in ABAQUS) were used for CSF, grey, and white matter in explicit dynamic analyses. Total hourglass

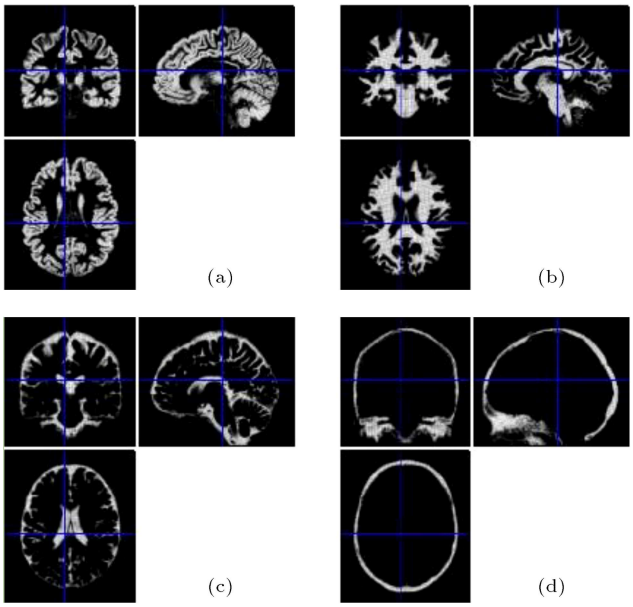

Figure 1. Post-image processing segmentation of tissue by using SPM 12: (a) Grey matter, (b) white matter, (c) cerebro-spinal fluid, and (d) skull.

Table 1. Number of elements in voxel-based Finite Element (FE) models generated with four different voxel resolutions.

Revolution (voxel size (mm))	No. of Hexahedral elements				
	Skull	CSF	Grey matter	White matter	Total
1	115010	42831	159301	120921	438063
1.5	75991	28563	106213	80599	291366
2	57387	21410	79635	60475	218907
4	27963	10723	39802	30221	108709

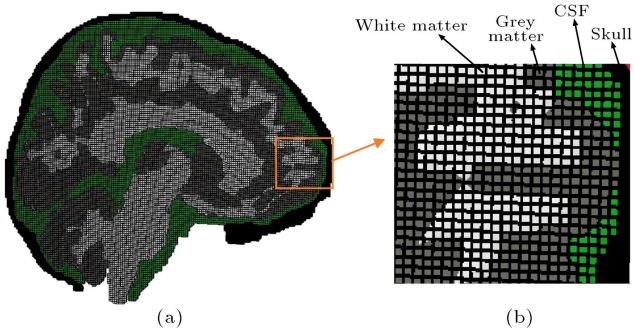

Figure 2. 2D view of the parasagittal slice of the assembly model (1 mm voxel resolution) showing morphological details and voxel boundaries between adjacent regions skull (black), CSF (green), grey matter (grey), and white matter (white).

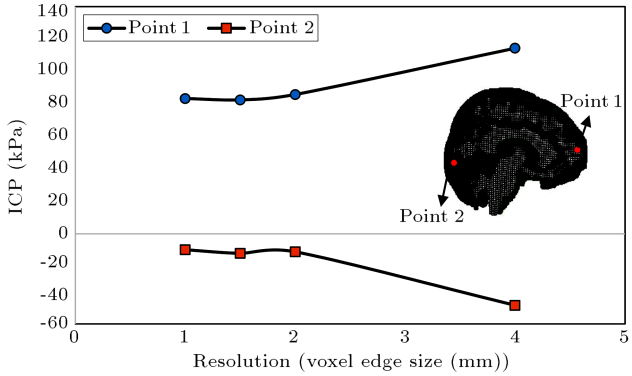

Figure 3. Variation of the maximum pressure at two points with the voxel resolution of the model.

energy was checked at every step to be lower than 10% of the peak internal energy at deformable parts of the model (i.e. CSF, grey matter, white matter). Mass scaling was applied to elements whose stable time increments were less than 1e-5 seconds at the beginning of each step. The percentage change in total model mass caused by mass scaling was checked to be less than 2% during every analysis. Skull elements were modelled as rigid. CSF was modelled with incompressible linear elastic behavior, with a density of 1 kg/m^3 and bulk modulus of 2.1 GPa [30]. A parasagittal slice of the model is shown in Figure 2.

In order to examine the effect of the grid size on the response of the FE model, four realizations of the model with linear elastic material properties and variable voxel size (in the range of 1–4 mm) were subjected to an anterior-posterior acceleration of 500 m/s^2 in 15 milliseconds. The maximum intracranial pressure (ICP) was measured at two nodes, one in the frontal lobe and one in the occipital lobe, as shown in Figure 3. The results indicated that the voxel size of 2 mm was sufficiently fine to stabilize the pressure at both points. Based on the results of Figure 9, the voxel-based FE model with element size of 2 mm was used to validate

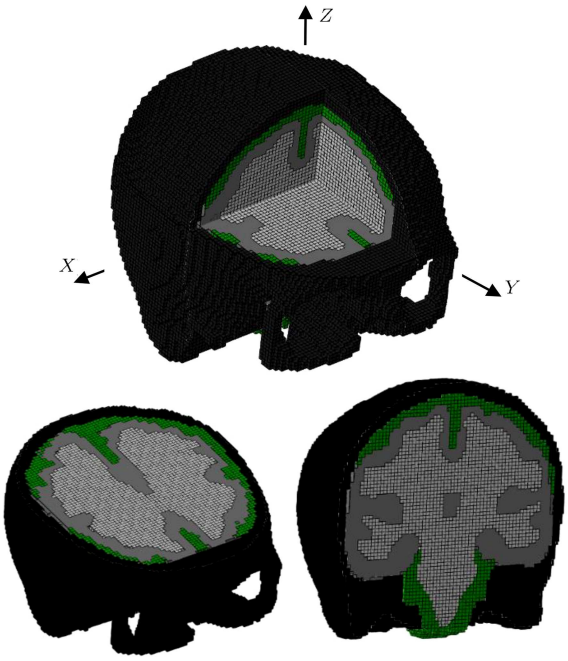

Figure 4. 3D sectional view of the voxel-based assembly of human head Finite Element (FE) model (SUTHM) with hexahedral cubic elements of skull, CSF, grey matter and white matter.

the model. A sectioned 3D representation of the model is shown in Figure 4.

2.3. Material properties

A wide variety of material properties have been proposed and applied to human brain FE models, ranging from linear elastic to viscoelastic and hyper-viscoelastic constitutive models. However, few hyperelastic models have the capacity to account for anisotropy at the sub-tissue level of the human brain. In this study, a hyperelastic model based on the Holzapfel-Gasser-Ogden (HGO) strain energy function was used [33]. This model has been recently generalized to account for fiber dispersion in the white matter [34].

2.3.1. Hyper elastic constitutive model

The general form of the HGO function may be written as:

$$W = \frac{G}{2}\left(\bar{I}_1 - 3\right) + K\left(\frac{J^2-1}{4} - \frac{1}{2}\ln J\right) + \frac{k_1}{2k_2}\sum_{i=1}^{N}\left(e^{k_2\langle\bar{E}_i\rangle^2} - 1\right), \quad (2)$$

where W denotes the strain energy per unit volume, and G and K represent the shear and bulk moduli, respectively. N is the number of existing fiber families in the fiber-matrix composite model, $\bar{I}_1$ is the first invariant of the isochoric Cauchy-Green deformation tensor, and $J = \det(F)$ is the volume ratio. $\bar{E}_i$

represents the strain in the direction of the ith fiber bundle (i.e. axonal bundle) defined as:

$$\bar{E}_i = \kappa\left(\bar{I}_1 - 3\right) + (1 - 3\kappa)\left(\overline{I_{4i}} - 1\right), \quad (3)$$

where, $\overline{I_{4i}} = \bar{C} : \vec{n}_{0i}\vec{n}_{0i}$, $\bar{C} = J^{\frac{-2}{3}}C$ is the isochoric part of the right Cauchy-Green deformation tensor and $\vec{n}_{0i}$ is the unit vector of fiber direction in the reference (undeformed) coordinate system. κ is a material parameter describing the dispersion of the fiber orientations around the main fiber direction $\vec{n}_{0i}$ (zero for fully aligned fibers denoting full transverse isotropy and $\frac{1}{3}$ for isotropic orientation denoting randomly oriented fibers). The Macaulay brackets cause $\bar{E}_i$ to become zero, in case its value is negative, and thus the fibers do not contribute to compression.

Assuming a single direction for fibers in the above equation and neglecting the nonlinear stiffness effects of the fiber ($k_2 \to 0$), Eq. (2) is reduced to:

$$W = \frac{G}{2}\left(\bar{I}_1 - 3\right) + K\left(\frac{J^2 - 1}{4} - \frac{1}{2}\ln J\right) + \frac{k_1}{2}\left\langle \bar{E}_1 \right\rangle^2. \quad (4)$$

In this study, the HGO constitutive model was used for both white and grey matter, with a difference wherein the grey matter is assumed to have isotopically oriented fibers (i.e. $\kappa = \frac{1}{3}$), while the dispersion of fibers within the voxels of white matter are assigned from DTI data using a discrete field. The bulk modulus is assumed constant and equal to 2.19 GPa for the brain and CSF. Based on previous studies, three candidate sets of hyperplastic parameters were generated. The first set of parameters (the "Low Modulus" parameter set) was obtained by fitting the HGO model to the tensile experiment results by Velardi et al. [20]. The fitting procedure is further described in a study by Wright and Ramesh [35]. The long-term shear moduli and fiber reinforcement parameter were reported as $\mu = 286$ Pa and $k_1 = 121$ Pa, respectively. As the tests were conducted at relatively low strain rate, the moduli were assumed to represent long-term behavior. A long-term to short-term shear moduli ration of 0.16 was used from Zhang et al. [6] to derive the instantaneous shear moduli and fiber reinforcement parameter.

The "High Modulus" set of parameters were obtained from the optimal fit of the HGO model to a tensile-compressive experiment on white matter samples at a higher strain rate of 30/s [22]. The average instantaneous shear modulus was reported by Hoursan et al. [36] as $\mu = 2210$ Pa. The ratio of fiber reinforcement parameter to shear moduli was assumed constant and equal to the average modulus. The "Average Modulus" was considered as the average of high and low moduli in terms of shear modulus. The ratio k_1/μ was considered equal to those of high and low moduli parameter sets. Fiber contribution to the stiffness was assumed linear (i.e. $k_2 \to 0$). The material parameters are displayed in Table 2.

In order to include the anisotropy data of axonal tracts into the model, the voxel-based implicit method has been employed rather than the explicit embedment of axonal tract structures [16]. A series of MATLAB scripts were used to calculate the dispersion parameter (representing the heterogeneity) and elemental orientation (representing anisotropy) for each element of the white matter. For each voxel (corresponding to a single hexahedral element), the position vector p in the global coordinate system was obtained from the T1 image, and the diffusion tensor of the corresponding voxel was extracted. Next, the diffusion tensor was diagonalized using Eigen decomposition. Subsequently, in order to obtain the dispersion parameter κ (representing heterogeneity), the eigenvalues were used to calculate FA (Eq. (5)). The dispersion parameter κ is then calculated from FA (Eq. (6)), further explained in Giordano and Kleiven [11] and written into the elemental dispersion matrix. On the other hand, the eigenvector corresponding to the highest eigenvalue

Table 2. Three sets of hyperelastic material parameters for grey and white matter regions of the SUTHM model.

		ρ (kg/m^3)	K (GPa)	μ_0 (Pa)	μ_∞ (Pa)	k_{10} (Pa)	$k_{1\infty}$ (Pa)	k_2 (Pa)	κ
High modulus	White matter	1040	2.19	2210	420	935	179	0.0001	From DTI
	Grey matter	1040	2.19	2210	420	935	179	0.0001	1/3
Average modulus	White matter	1040	2.19	1865	353	786	150	0.0001	From DTI
	Grey matter	1040	2.19	1865	353	786	150	0.0001	1/3
Low modulus	White matter	1040	2.19	1520	286	637	121	0.0001	From DTI
	Grey matter	1040	2.19	1520	286	637	121	0.0001	1/3

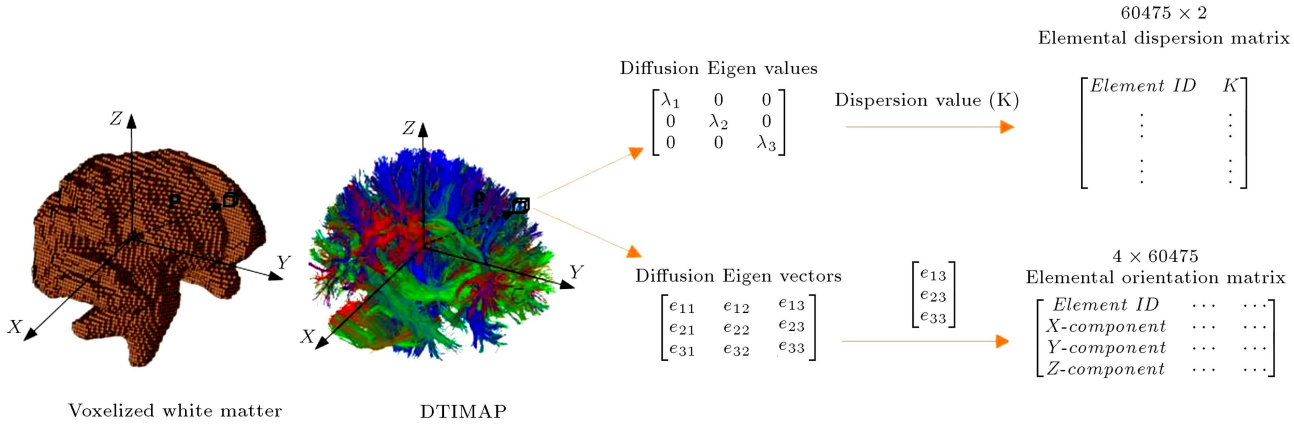

Figure 5. Schematic illustration of inclusion of anisotropy and heterogeneity into the voxel-based white matter of SUTHM. P is the position vector of a representative voxel in the white matter, corresponding to a single element in the Finite Element (FE) model. Elemental orientation and dispersion matrices are formed for white matter.

was considered as the main orientation of the fibers within the voxel and used to create the elemental orientation matrix. The obtained elemental orientation and dispersion matrices are finally written into the analysis input file via a custom python code. The procedure is illustrated in Figure 5.

$$FA = \sqrt{\frac{1}{2}}\sqrt{\frac{(\lambda_1-\lambda_2)^2+(\lambda_1-\lambda_3)^2+(\lambda_2-\lambda_3)^2}{\lambda_1^2+\lambda_2^2+\lambda_3^2}}, \tag{5}$$

$$\kappa = \frac{1}{2}\frac{-6+4FA^2+2\sqrt{3FA^2-2FA^4}}{-9+6FA^2}. \tag{6}$$

2.3.2. Viscoelastic behaviour

In order to incorporate viscoelasticity, a Quasi-Linear Viscoelastic (QLV) model was used, as proposed by Fung [37]. Assuming the time-dependent behavior to be given by a Prony Series, the stress can be written in the following form [25]:

$$S(t) = \int_0^t \left[M_0 - \sum_i M_i e^{\left(-\frac{t-p}{\tau_i}\right)}\right]\frac{dS_e}{dp}dp, \tag{7}$$

where p is a time variable that spans from initial time to current time, S_e is the deviatoric elastic stress, and M_0 is the instantaneous material parameters G and k_1. M_i and τ_i are time dependent coefficients obtained from material response in a relaxation test. Here, the constants proposed by Cloots et al. [25] were used, as shown in Table 3.

3. Model validation

3.1. Nahum's impact

Simulation results of the SUTHM are compared with the intracranial pressure-time recordings from experiment no. 37 conducted by Nahum et al. [2], where the forehead of the cadaver, inclined forward by 45 degrees, was impacted by a padded impactor. The acceleration pulse resulting from the force measured upon the impact was applied to the skull (Figure 6). The intracranial pressure-time curves in the frontal and occipital regions from this experiment were compared to the predictions of models with different material properties.

Table 3. The proposed viscoelastic parameters of axon and ECM in brain white matter [25].

M_1 for $\tau_1 = 10^{-6}$ s	0.7685
M_2 for $\tau_1 = 10^{-5}$ s	0.1856
M_3 for $\tau_1 = 10^{-4}$ s	0.0148
M_4 for $\tau_1 = 10^{-3}$ s	0.0190
M_5 for $\tau_1 = 10^{-2}$ s	0.0026
M_6 for $\tau_1 = 10^{-1}$ s	0.0070
M_∞	0.0025

3.2. Relative motion between the skull and brain

A test of relative motion between the brain and the skull was performed based on the experimental data presented by Hardy et al. [3] and King et al. [38], which describes the relative displacement between the brain and skull of a human cadaver, using a high-speed biplane x-ray system and Neutral Density Targets (NDTs). In the experiment, cylinders of 3.9 mm length and 2.3 mm diameter were used as NDTs, implanted in two vertical columns located in the occipitoparietal and temporoparietal regions, spaced approximately 10 mm apart (Figure 7). The cadaver head was inverted and suspended in a fixture that allowed rotation and translation. The NDT's numbered "a_6"and "p_6" were located in the brain toward the apex of the skull, while the "a_1" and "p_1" were located just above the

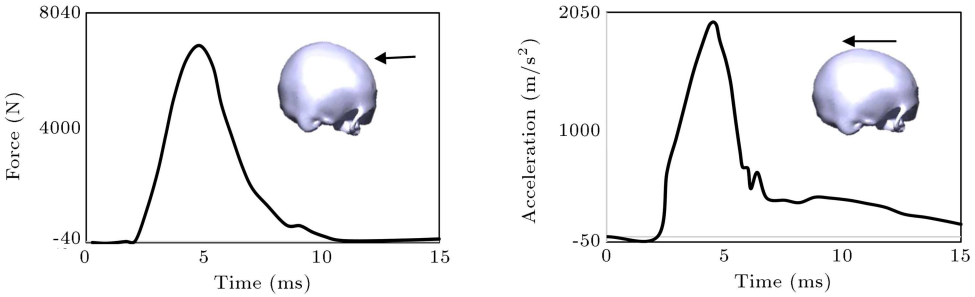

Figure 6. Frontal head impact from the cadaver experiment no. 37 by Nahum et al. [2]. Force measurement (left) and head acceleration (right).

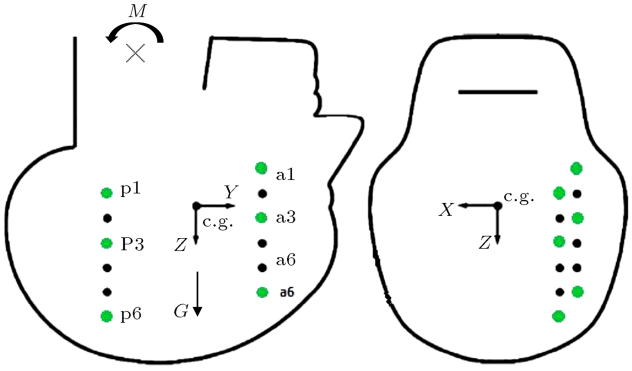

Figure 7. Schematic of suspended head and NDT locations from experiment C383-T1 [38]. The green NDT locations have been chosen for analysis in the current study. The Y-relative displacement was measured during simulation at a_1, a_3, a_6, p_1, p_3, and p_6 locations.

base of the skull (Figure 7). Experiment C383-T1 was simulated, which evaluates anterior-posterior relative displacements when the cadaver is subjected to a frontal impact described by the acceleration pulse of Figure 8. The relative displacement was measured at 6 locations in the FE model corresponding to 6 NDT locations from the experiment (i.e. a_1, a_3, a_6, p_1, p_3, p_6, as shown in Figure 7). In order to replicate experimental conditions, the model was hinged at the skull base (neck joint) with 80 N/m rotational stiffness [3] and subjected to a constant gravitational acceleration of 10 m/s^2 in the $+z$ direction (inverted suspended cadaver). The absolute Y-displacement at each NDT point was measured relative to a certain point at the base of the skull.

4. Results

The results of the simulation of Nahum's impact are shown in Figure 9. The predicted response in terms of the ICP was recorded at two nodes in the frontal and occipital lobes. The results are indicated for three sets of material parameters in Figure 10. It was observed that, while the three sets of material parameters resulted in 0.5–3 ms earlier pressure peaks than those of the experimental curves, the high modulus model displayed better agreement with the experimental results, especially at the occipital lobe. The frontal and occipital peak pressure magnitudes were only 8%, and 6% higher than those of the experiment, respectively. In addition, tensile resistance at the occipital lobe, due to the tie constraint at the brain-skull boundary, is well reflected in the negative pressures at the occipital lobe (Figure 2(b)). This can also be inferred from temporal evolution of ICP gradients within the brain. As observed in the contour plots of Figure 10, the first wave of pressure propagates upon impact (t = 0 ms), causing almost simultaneous positive (coup) and negative (countercoup) values of pressure at frontal and occipital lobes, respectively. The second pressure

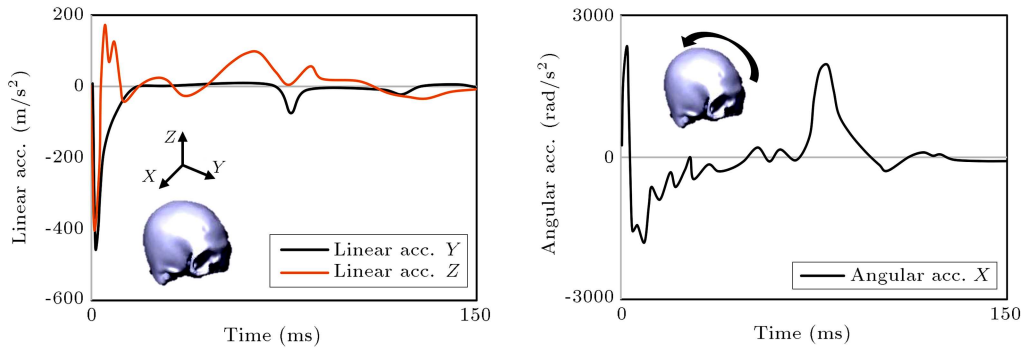

Figure 8. Acceleration pulse applied by King et al. [38], C383-T1 frontal impact.

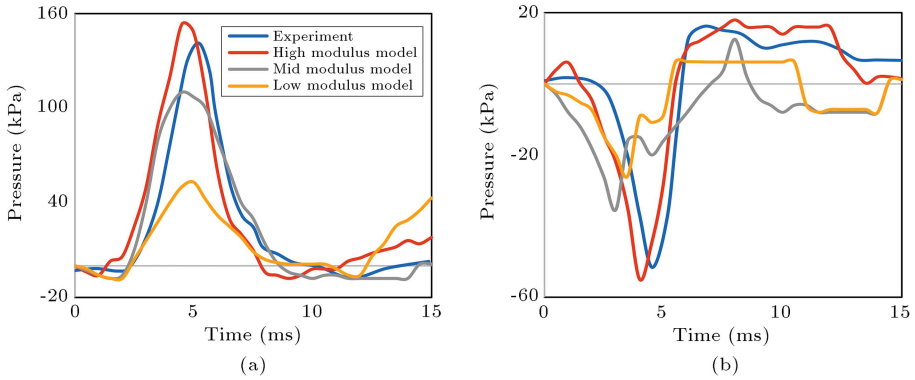

Figure 9. Simulation of intracranial pressure results from the cadaver experiment of Nahum et al. (1977) applied to the SUTHM model with three sets of material parameters: (a) Frontal lobe pressure and (b) occipital lobe pressure.

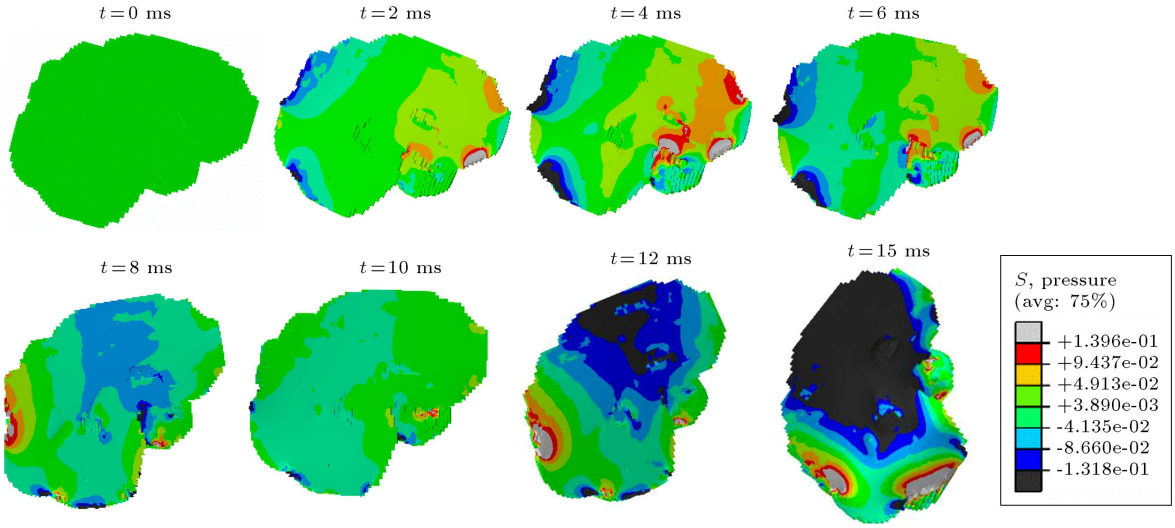

Figure 10. Deformed configurations and contour plots of intracranial pressure within the brain during the simulation of Nahum's frontal impact (SUTHM with high modulus parameter set).

wave, characterized by negative ICP at the impact site (frontal lobe) and positive ICP on the opposite side of the impact site (occipital lobe), propagates after the collision and damping of the first wave ($t \geq 10$ ms).

The results for the relative displacement in Y-direction are displayed in Figure 11 for 6 locations in the occipitoparietal and temporoparietal regions of the SUTHM model. As expected, the magnitude of the relative motion in the NDT points increases with decreasing stiffness. In particular, the low modulus set the highest positive and negative peaks of displacement at all NDT locations, overestimating the experimental maxima and minima by an average of 72 percent. On the other hand, under the stiffest set of material properties (i.e. high modulus parameter set), the maxima and minima were underestimated by an average of 40 percent for relative displacement in the Y-direction. An average delay of 5 ms was observed at the peaks of model-predicted data, with respect to the experimental data. In particular, the most compliant model (i.e. low modulus parameter set) displayed 10 ms and 20 ms delay in the first peak at a_1 and a_3 locations.

In order to compare the model performance against the previously published models, the CORA rating method was used to evaluate the similarity of the model-predicted and experimental curves using two independent sub-rating methods: a corridor method and a cross correlation method [39]. The CORA scores of the current model with three different sets of material parameters were compared against the CORA ratings published for other human FE head models for relative motion in a Y-direction under frontal C383-T1 impact (Figure 12). The previously published models considered here include the DHIM (Dartmouth Head Injury Model [40]), KTH (Kungliga Tekniska Högskolan [8,29]), GHBMC (Global Human Body Models Consortium [7]), SIMon (Simulated Injury Monitor [9]), and ABM (ATLAS-based Brain Model [5]). A CORA rating of 1 indicates a perfect match of the curves.

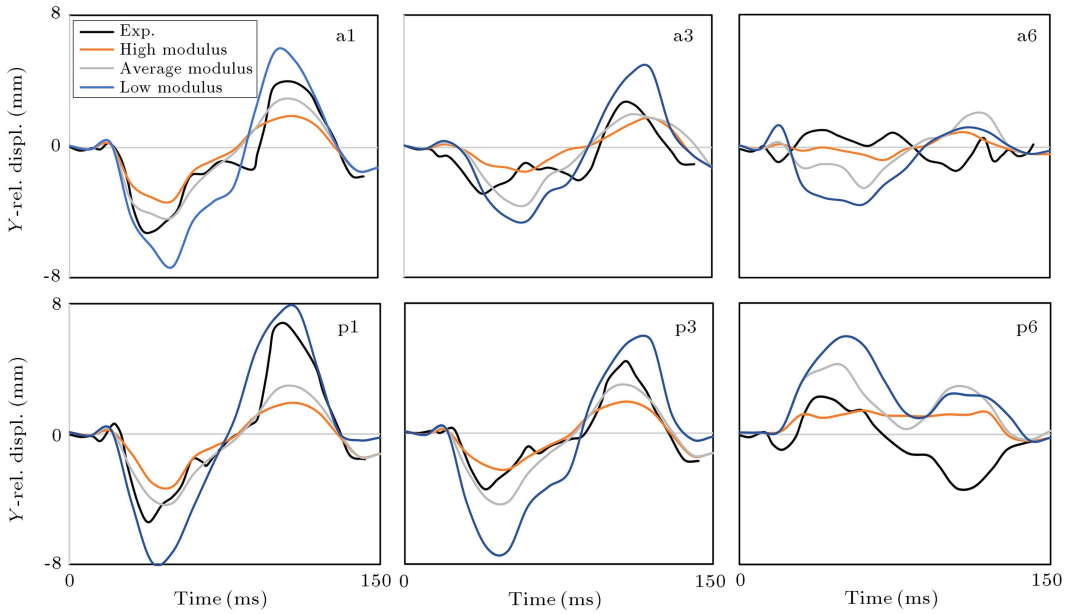

Figure 11. Simulation of relative skull-brain motion for the frontal impact C383-T1. For marker locations and coordinate system directions, see Hardy et al. (2001) [3]. Experimental data (black curves) are plotted together with the anisotropic model responses (colored lines).

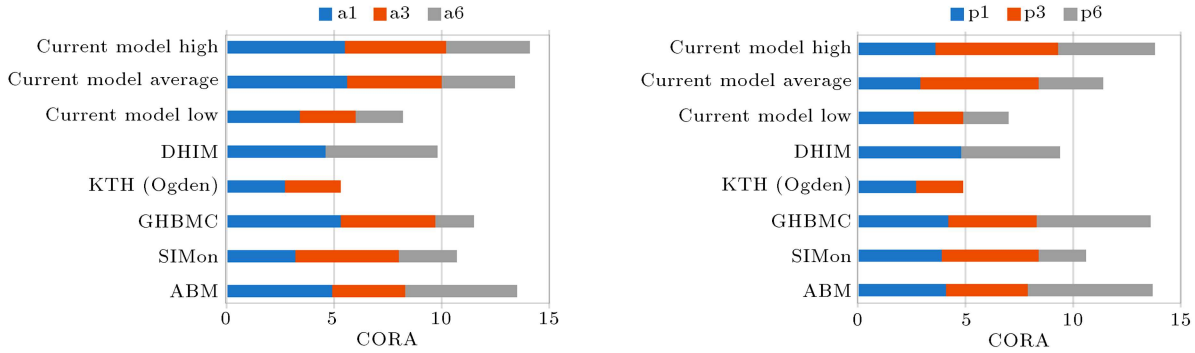

Figure 12. CORA analysis result of similarity between the curves obtained from different models in the relative motion test by comparing the present model findings with those of previous models.

5. Discussion

A novel 3D FE human head model with enhanced computational cost was developed from MR Imaging data using a voxel-based mesh generation algorithm. The anisotropy and heterogeneity of material properties within the white matter were introduced into the model using a direct one-to-one correspondence between the FEs and voxel-based diffusion data. In order to insert the diffusion information into the white matter, the DTI voxel belonging to a single FE of the brain was identified based on spatial coordinates, and the diffusion information was derived from the diffusion matrix, directly. In previous anisotropic models, due to the incompatibility of DTI data and FE mesh, the diffusion information was averaged to extract the mean element anisotropy information considering the normalized distance from the center of the voxel to the center of the FE for each selected voxel [11,24]. The anisotropic SUTHM model presented here offers refined mesh with more local accuracy which avoids the systematic loss of information due to averaging. In addition, the current model achieved a relatively lower computational cost by investigating the influence of mesh resolution on the pressure response of the model.

Simulation of intra-cranial pressure at two locations in the frontal and occipital lobe subjected to Nahum's impact shows the model predictions are highly dependent on the choice of constitutive material properties. The high modulus parameter set exhibited the strongest agreement with experimental data, with the frontal and occipital peak pressure magnitudes only 8% and 6% higher than those of the experiment, while the low modulus set displayed the weakest correlation with peak pressures 51% and 31% lower than those of the experiment at frontal and occipital lobes, re-

spectively. The maximum ICP of the high modulus set was 153 kPa at coup site, slightly higher than that of the experimental curve (141 kPa), while the most compliant set (low modulus) displayed the peak pressure of only 50 kPa. In addition, while the high modulus material set peaked simultaneously with the experimental curve at the countercoup site (negative pressure), the negative pressure peak of the average modulus parameter set occurred 2 ms earlier. The patterns of pressure wave propagation at coup and countercoup sites were similar to previous observations in terms of pressure changes within the tissue [41]. In particular, the irregular trauma distribution reported in coup and countercoup injuries [42] may be explained by dynamic pressure transients observed to be carried around the skull by flexural waves [43], from coup to countercoup.

The important effects of tissue compliance, reflected in the constitutive material properties, were also found in the simulation of the relative displacement between the brain and skull. There was considerable difference between the responses of the SUTHM with different sets of material properties, especially at occipitoparietal NDT locations (i.e. p_1-p_3-p_6). It was observed that, while several models can capture the experimentally measured relative motions, the SUTHM model with the high-modulus parameter set has the highest overall CORA score (marginally higher than the ABM model) for three temporoparietal NDTs (a_1, a_3, a_6), while the average-modulus model has the third place (slightly below the ABM model). Furthermore, while all models perform relatively well at the a_1 location, there is a considerable difference across the CORA scores at the a_6 location with the DHIM model exhibiting the best response with a CORA score of 0.52. In addition the CORA scores at occipitoparietal NDT locations (p_1, p_3, p_6) are marginally lower in almost all models, where the highest overall score goes to GMBHC, ABM, and SUTHM with high modulus parameter sets, at almost equal values. On the other hand, the previously proposed models displayed considerable variation of CORA score across different locations. For instance, the GMBHC response at three temporoparietal NDTs range from the CORA score of 0.53 at a_1 to 0.18 at a_6. However, the CORA scores of our SUTHM model displayed less variation across different locations (0.39–0.55 at temporoparietal and 0.36–0.57 at occipitoparietal NDT locations), indicating more reliability.

Finally, although the voxel-based SUTHM model presented in the current study exhibited better results compared to previous models in terms of the Y-relative displacement, it remains to be studied under impact in other directions, as well as rotational accelerations, in the future. In addition, although the effect of neck flexural stiffness was modelled in the course of analyses, the presence of neck tissue in the FE model has been shown to have important effects, especially in case of rotational accelerations. In particular, Newman et al. [44] reported a minimal effect of neck stiffness on linear accelerations but larger effects on rotational accelerations. Since the model was validated against linear accelerations in the current study, this effect was simplified with a fixed flexural moment applied to the base of the skull for the time being. However, the model remains to be validated under rotational accelerations in future studies. Furthermore, although the CSF-skull and CSF-brain boundary conditions were assessed in this study, the important effects of CSF geometry and material properties on the results remain to be investigated in future applications of the model. Finally, while previous studies have shown that the vasculature has a minimal biomechanical influence on the dynamic responses of the brain in a 3D FE head model [30,45], it can be simulated in order to account for the damage to vessels as the result of the strain field in TBI.

Acknowledgment

This research has been supported by the INSF (Iran National Science Foundation)

Nomenclature

W	Strain energy density (N.m)
G	Shear modulus (Pa)
E	Strain (-)
$\bar{I}$	Invariant of the deformation tensor (-)
$\bar{J}$	Volume ratio (-)
k_1	Fiber stiffness (Pa)
k_2	Nonlinear effects coefficient (-)
N	Number of fiber bundles (-)
C	Right Cauchy-Green deformation tensor (-)
K	Bulk modulus (Pa)
λ	Eigenvalue of diffusion tensor (-)
FA	Fractional Anisotropy (-)
S	Stress tensor (Pa)
M	Material parameter (-)
$\vec{n}_i$	Unit vector of fiber direction (-)
κ	Material parameter for dispersion (-)

References

1. Galgano, M., Toshkezi, G., Qiu, X., Russell, T., Chin, L., and Zhao, L.R. "Traumatic brain injury: Current treatment strategies and future endeavors",

Cell Transplantation, **26**(7), pp. 1118—1130 (2017). DOI:10.1177/0963689717714102

2. Nahum, A.M., Smith, R., and Ward, C.C. "Intracranial pressure dynamics during head impact", *SAE Technical Paper* (1977).
3. Hardy, W., Foster, C., Mason, M., Yang, K., King, A., and Tashman, S. "Investigation of head injury mechanisms using neutral density technology and high-speed biplanar X-ray", *Stapp Car Crash J.*, **45**, pp. 337–368 (2001).
4. Hardy, W., Mason, M., Foster, C., Shah, C., Kopacz, J., Yang, K., King, A., Bishop, J., Bey, M., Anderst, W., and Tashman, S. "Study of the response of the human cadaver head to impact", *Stapp Car Crash J.*, **51**, pp. 17–80 (2007).
5. Miller, L.E., Urban, J., and Stitzel, J.D. "An anatomically accurate finite element brain model: development, validation and comparison to existing models" (2016).
6. Zhang, L.Y., Yang, K.H., and King, A.I. "A proposed injury threshold for introduction mild traumatic brain injury", *J. Biomech. Eng.*, **126**, pp. 226–236 (2004).
7. Mao, H., Zhang, L., Yang, K.H., and King, A.I. "Application of a finite element model of the brain to study traumatic brain injury mechanisms in the rat", *Stapp Car Crash J.*, **50**, pp. 583–600 (2006).
8. Kleiven, S. "Predictors for traumatic brain injuries evaluated through accident reconstructions", *Stapp Car Crash J.*, **51**, pp. 81–114 (2007).
9. Takhounts, E., Hasija, V., Ridella, S., et al. "Investigation of traumatic brain injury using the next generation of simulated injury monitor (simon) finite element head model", *Stapp Car Crash J.*, **52**, pp. 1–32 (2008).
10. Hoursan, H., Ahmadian, M.T., and Naghibi Beidokhti, H. "Modelling and analysis of the effect of angular velocity and acceleration on brain strain field in traumatic brain injury", *ASME 2013 International Mechanical Engineering Congress & Exposition IMECE2013* (2013).
11. Giordano, C., Cloots, R., van Dommelen, J., Kleiven, S., and Geers, M. "The influence of anisotropy on brain injury prediction", *J. Biomech.*, **47**, pp. 1052–1059 (2014). Doi: 10.1016/j. jbiomech.2013.12.036
12. Shafiee, A., Ahmadian, M.T., Hoursan, H., and Hoviat Talab, M. "Effect of linear and rotational acceleration on human brain", *Modares Mechanical Engineering*, **15**(7), pp. 248–260 (2015).
13. Hoursan, H., Ahmadian, M.T., Kazemiasfeh, R., and Barari, A. "On the validity extent of linear viscoelastic models of human brain", *CSME-SCGM2018* (2018).
14. Afshari, J., Haghpanahi, M., Kalantarinejad, R., and Rouboa, A. "Investigating the effects of impact directions to improve head injury index", *Scientia Iranica, Trans. B*, **27**(4), pp. 1867–1877 (2019).
15. Razaghi, R., Biglari., H., and Karimi, A. "Risk of rupture of the cerebral aneurysm in relation to traumatic brain injury using a patient-specific fluid-structure interaction model", *Computer Methods and Programs in Biomedicine*, **176**, pp. 9–16 (2019). DOI: 10.1016/j.cmpb.2019.04.015
16. Hajiaghamemar, M., Wu, T., Panzer, M.B., and Margulies, S.S. "Embedded axonal fiber tracts improve finite element model predictions of traumatic brain injury", *Biomech Model Mechanobiol*, **19**(3), pp. 1109–1130 (2020). DOI: 10.1007/s10237-019-01273-8
17. Hoursan, H., Farahmand, F., and Ahmadian, M.T. "A three-dimensional statistical volume element for histology informed micromechanical modeling of brain white matter", *Annals of Biomedical Engineering*, **48**(4), pp. 1337–1353 (2020).
18. Leemans, A., Jeurissen, B., Sijbers, J., and Jones, D.K. "Explore DTI: A graphical toolbox for processing, analyzing, and visualizing diffusion MR data", In *17th Annual Meeting of Intl Soc. Mag Reson. Med.*, p. 3537, Hawaii, USA (2009).
19. Sepehrband, F., Alexander, C.D., Clark, K.A., Kurniawan, N.D., Yang, Z., and Reutens, D.C. "Parametric probability distribution functions for axon diameters of corpus callosum", *Front. Neuroanat*, **10**, p. 59 (2016).
20. Velardi, F., Fraternali, F., and Angelillo, M. "Anisotropic constitutive equations and experimental tensile behavior of brain tissue", *Biomech. Model. Mechanobiol.*, **5**, pp. 53–61 (2006).
21. Rashid, B., Destrade, M., and Gilchrist, M. "Mechanical characterization of brain tissue in tension at dynamic strain rates", *Journal of the Mechanical Behavior of Biomedical Materials*, **33**, pp. 43–54 (2012). 10.1016/j.jmbbm.2012.07.015
22. Jin, X., Zhu, F., Mao, H., Shen, M.C., and Yang, K.H. "A comprehensive experimental study on material properties of human brain tissue", *Journal of Biomechanics*, **46**(16), pp. 2795–801 (2013).
23. Budday, S., Sommer, G., Holzapfel, G.A., Steinmann, P., and Kuhl, E. "Viscoelastic parameter identification of human brain tissue", *Journal of the Mechanical Behavior of Biomedical Materials*, **74**, pp. 463–476, ISSN 1751-6161 (2017).
24. Giordano, C., Zappalà, S., and Kleiven, S. "Anisotropic finite element models for brain injury prediction: the sensitivity of axonal strain to white matter tract inter-subject variability", *Biomechanics and Modeling in Mechanobiology*, **16**, pp. 1269–1293 (2017). DOI:10.1007/s10237-017-0887-5
25. Cloots, R.J., van Dommelen, J.A., Nyberg, T., Kleiven, S., and Geers, M.G. "Micromechanics of diffuse axonal injury: Influence of axonal orientation and anisotropy", *Biomech Model Mechanobiol*, **10**(3), pp. 413–422 (2011). DOI: 10.1007/s10237-010-0243-5. Epub 2010 Jul 16. PMID: 20635116.

26. Zhou, Z, Li, X, and Kleiven, S. "Biomechanics of acute subdural hematoma in the elderly: A fluid-structure interaction study", *J Neurotrauma*, **36**(13), pp. 2099–2108 (2019). DOI: 10.1089/neu.2018.6143. Epub 2019 Mar 13. PMID: 30717617.

27. Fernandes, F., Tchepel, D., Alves de Sousa, R., and Ptak, M. "Development and validation of a new finite element human head model", *Engineering Computations*, **35**(1), pp. 477–496 (2018). https://doi.org/10.1108/EC-09-2016-0321

28. Saboori, P. and Sadegh, A. "Material modeling of the head's subarachnoid space", *Scientia Iranica*, **18**(6), pp. 1492–1499, ISSN 1026-3098 (2011).

29. Kleiven, S. and von Holst, H. "Consequences of head size following trauma to the human head", *J. Biomech.*, **35**, pp. 153–160 (2002)

30. Johnson, H., von Holst, H., and Kleiven, S. "Automatic generation and validation of patient-specific finite element head models suitable for crashworthiness analysis", *International Journal of Crashworthiness*, **14**(6), pp. 555–563 (2009). DOI: 10.1080/13588260902895708

31. Karimi, A., Rahmati, S.M., and Razaghi, R. "A combination of experimental measurement, constitutive damage model, and diffusion tensor imaging to characterize the mechanical properties of the human brain", *Comput Methods Biomech Biomed Engin.*, **20**(12), pp. 1350-1363 (2017). DOI:10.1080/10255842.2017.1362694

32. Reuter M., Schmansky, N.J., Rosas, H.D., and Fischl, B. "Within-subject template estimation for unbiased longitudinal image analysis", *Neuroimage*, **61**(4), pp. 1402–1418 (2012).

33. Holzapfel, G.A., Gasser, T.C., and Ogden, R.W. "A new constitutive framework for arterial wall mechanics and a comparative study of material models", *Journal of Elasticity*, **61**, pp. 1–48 (2000).

34. Carlsen, R.W. and Daphalapurkar, N.P. "The importance of structural anisotropy in computational models of traumatic brain injury", *Front Neurol.*, **6**(28), pp. 6–28 (2015). DOI: 10.3389/fneur.2015.00028

35. Wright, R.M. and Ramesh, K.T. "An axonal strain injury criterion for traumatic brain injury", *Biomech. Model. Mechanobiol.*, **11**, pp. 245–260 (2012).

36. Hoursan, H., Farahmand, F., and Ahmadian, M.A. "Novel procedure for micromechanical characterization of white matter constituents at various strain rates", *Scientia Iranica, Transactions on Mechanical Engineering (B)*, **27**(2), pp. 784–794 (2020). DOI: 10.24200/sci.2018.50940.1928

37. Fung, Y., *Biomechanics: Mechanical Properties of Living Tissues*, Springer-Verlag, New York (1981).

38. King, A.I., Yang, K.H., Zhang, L., Hardy, W., and Viano, D.C., *Is Head Injury Caused by Linear or Angular Acceleration*, Bioengineering Center, Wayne State University, pp. 1–12 (2003).

39. Gehre, C., Gades, H., and Wernicke, P. "Objective rating of signals using test and simulation responses", *Pap. Present 21st ESV Conf.* (Jun 15, 2009).

40. Ji, S., Ghadyani, H., Bolander, R.P., et al. "Parametric comparisons of intracranial mechanical responses from three validated finite element models of the human head", *Ann. Biomed. Eng. Jan.*, **42**(1), pp. 11–24 (2014).

41. Pearce, C.W. and Young, P.G. "On the pressure response in the brain due to short duration blunt impacts", *PloS One*, **9**(12), e114292 (2014). DOI:10.1371/journal.pone.0114292

42. Bhateja, A., Shukla, D., Devi, B.I., and Sastry Kolluri, V. "Coup and contrecoup head injuries: Predictors of outcome", *Indian. J. Neurotrauma*, **6**, pp. 115–118 (2009).

43. Hoursan, H. and Ahmadian, M.T. "Dynamic behaviour of Ox tibial and femoral bones: A comparison with human bones", *Proceedings of the ASME 2015 International Design Engineering Technical Conferences and Computers and Information in Engineering Conference*, **8**, *27th Conference on Mechanical Vibration and Noise*, Boston, Massachusetts, USA, V008T13A053, ASME (2015). https://doi.org/10.1115/DETC2015-46555

44. Newman, J.A., Beusenberg, M.C., Shewchenko, N., Withnallm, C., and Fournier, E. "Verification of biomechanical methods employed in a comprehensive study of mild traumatic brain injury and the effectiveness of American football helmets", *J. Biomech.*, **38**(7), pp. 1469–1481 (2005).

45. Johnson, H. and Kleiven, S. "Dynamic response of the brain with vasculature: a three-dimensional computational study", *Journal of Biomechanics*, **40**(13), pp. 3006–12 (2007).

Biographies

Hesam Hoursan obtained his MS degree in the field of traumatic brain injury and multi-scale modelling of soft tissue and is currently a PhD graduate student at Sharif University of Technology, Iran, working in the same field. He has also published several articles in this area of study. His current research focus is multi-scale modelling including macro-micro scale integration in TBI.

Farzam Farahmand is Professor of Biomechanics and Deputy of Technology at Sharif University of Technology, Tehran, Iran. He is Director of the Dr. Javad Mowafaghian Research Center of Neuro-Rehabilitation Technologies, Tehran, Iran, and Director of the Surgical Robotics Laboratory at the Research Center of Biomedical Technologies Robotics (RCBTR) in Tehran University of Medical Sciences, Tehran, Iran. His

main areas of interest include orthopedic biomechanics, rehabilitation and soft tissues.

Mohammad Taghi Ahmadian received his BS and MS degrees in Physics from Shiraz University, Iran. He completed the requirements for BS and MS degrees in Mechanical Engineering in 1980 from the University of Kansas in Lawrence from where he also obtained a PhD in Physics and a PhD in Mechanical Engineering in 1981 and 1986, respectively. His research interests are micro and nano mechanics as well as bioengineering. He has recently focused on brain and TBI phenomena as hyper-visco elastic soft tissues.

Sadegh Masjoudi is a PhD graduate in the Department of Medical Physics and Biomedical Engineering, Tehran University of Medical Sciences. He has completed several research papers and publications in the field of brain image processing and fiber tractography mapping.